Applied Catalysis B: Environmental 172–173 (2015) 91–99

Contents lists available at ScienceDirect

Applied Catalysis B: Environmental

journal homepage: www.elsevier.com/locate/apcatb

Controllable synthesis of highly active BiOCl hierarchical microsphere self-assembled by nanosheets with tunable thickness

Liyong Ding, Renjie Wei, Huan Chen, Juncheng Hu*, Jinlin Li

Key Laboratory of Catalysis and Materials Science of the State Ethnic Affairs Commission & Ministry of Education, South-Central University for Nationalities, Wuhan 430074, PR China

ARTICLE INFO

Article history:
Received 24 December 2014
Received in revised form 9 February 2015
Accepted 14 February 2015
Available online 17 February 2015

Keywords:
Microsphere
BiOCl
Nanosheets
Thickness
Photocatalysis

ABSTRACT

Uniform BiOCl hierarchical microspheres assembled by nanosheets with tunable thickness were synthesized via a simple solvothermal route. XRD, SEM, TEM, XPS, BET, UV–vis and DRS were performed to investigate the structural and optical properties of the samples. The results indicated that the morphology and structure of the BiOCl could be controlled by adjusting the pH values. With the increase of the amount of ammonia solution, the thickness of assembled nanosheets became thinner from 50 nm to 10 nm or even less than 10 nm. The specific surface area of BiOCl hierarchical microspheres increased as well. The influence of different pH value on the performance of BiOCl hierarchical microsphere was studied systematically. All the BiOCl hierarchical microspheres showed higher photocatalytic activities for the RhB degradation than commercial P25 under visible light irradiation. The sample obtained at pH 5 showed the highest activity for dye photosensitization degradation of RhB under visible light irradiation due to the large specific surface area and considerable oxygen vacancies. Furthermore, the BiOCl hierarchical microspheres also exhibited high photocatalytic performance for the direct semiconductor photoexcitation degradation of salicylic acid and phenol under UV light irradiation.

1. Introduction

With the development of society and technology, energy shortages and environmental pollution have become the focus of attention of the word [1–4]. As one of the most promising solutions for these problems, semiconductor photocatalytic technology has recently drawn much attention, since it is one of the most effective and green method for decomposing water into hydrogen [5,6], decomposing harmful pollutant [7] and converting CO_2 to energy-bearing carbon fuel sources [8]. Various semiconductor materials have been synthesized in the past few decades [9,10]. To date, TiO_2 semiconductor has been undoubtedly proven to be one of the excellent photocatalysts [11]. Unfortunately, its band gap (3.2 eV) is too wide to efficiently utilize of visible light. Aiming at developing visible-light-driven photocatalysts, researchers in numerous laboratories have focused on doping TiO_2 with foreign nonmetal or mental element [12], exposing facets [13], or using composite materials [14]. Nonetheless, adequate stability and practicability for utilizing visible light have not yet been fully realized.

Bismuth oxychloride (BiOCl) is a novel V–VI–VII ternary semiconductor compound crystallized in a tetragonal matlockite structure [15], with a layer structure characterized by $[Bi_2O_2]^{2+}$ slabs interleaved by double slabs of Cl ions (Fig. S1a). The formed intra-electric field along the [0 0 1] direction caused by $[Bi_2O_2]^{2+}$ layers and Cl atom layers can accelerate the transfer of the photo-induced carriers along the [0 0 1] direction [16]. It is well-known that the oxygen density on the (0 0 1) facets is much higher than that on the (1 1 0) facets (Fig. S1b and c), which is favorable for the adsorption of reactants [17]. Many researchers had demonstrated that BiOCl nanosheets with exposed {0 0 1} facets exhibited superior photocatalytic activity. For example, Jiang et al. [18] had reported BiOCl single-crystalline nanosheets with different exposed {0 0 1} and {0 1 0} facets exhibited different activity. Guan et al. [19] had recently achieved high solar photocatalytic activity in ultrathin BiOCl nanosheets with almost fully exposed active {0 0 1} facets. However, there are few literatures relevant to the thickness of nanosheets. Due to the highly anisotropic layered structures, BiOCl tends to grow into nanoplates/sheets with 2D features. Compared with 2D nanostructures, 3D assembled hierarchical architectures possess much unique properties, including improved light harvesting, faster interfacial charge separation, shortened diffusion pathways and more reactive sites [20], which can enhance photocatalytic activity significantly. Therefore,

* Corresponding author. Tel.: +86 27 67841302.
E-mail address: jchu@mail.scuec.edu.cn (J. Hu).

http://dx.doi.org/10.1016/j.apcatb.2015.02.019
0926-3373/

to obtain 3D BiOCl hierarchical microsphere with a high degree of reactive surface and a large surface area is an effective method.

In this work, uniform 3D microspherical BiOCl architectures assembled by nanosheets with tunable thickness were successfully synthesized by using a simple solvothermal route. During the process, acetic acid was used as cosolvent to facilitate the dissolution of bismuth nitrate, and ammonia solution was utilized to adjust the pH value to control the thickness of the nanosheets. The products were controllable synthesized with tunable thickness. The effect of the pH value on the thickness and photocatalytic activity of BiOCl was investigated in detail. With the increase of the pH values, the thickness of the nanosheets decreased. All the BiOCl hierarchical microspheres showed higher activities for the RhB degradation than commercial P25 under visible light irradiation. The BiOCl hierarchical microspheres obtained at pH 5 showed highest activity for dye photosensitization degradation of RhB and also exhibited high photocatalytic performance for the direct semiconductor photoexcitation degradation of salicylic acid and phenol.

2. Experimental

2.1. Preparation of BiOCl hierarchical microspheres

All of the chemicals were purchased from Sinopharm Chemical Reagent Co., Ltd. (Shanghai, China), analytical grade, and used as received without any further treatment.

In a typical synthesis procedure, 2.5 mmol $Bi(NO_3)_3{\cdot}5H_2O$ was first dissolved in 7.5 mL acetic acid. After complete dissolution, 60 mL methanol was added under vigorous stirring. Subsequently, 4.2 mL HCl (0.6mol L^{-1}) aqueous solution was added in drops, and a white suspension formed immediately. The different pH values of the solution (2, 4–8 and 10) were then adjusted using concentrated ammonia solution under smashing stirring. The mixture was stirred for another 0.5 h at room temperature in air, than was transferred to a 100 mL Teflon-lined stain-less steel autoclave, followed by heating and maintaining at 180 °C for 5 h, and then naturally cooled to ambient temperature. The resulting precipitates were washed with deionized water and ethanol thoroughly to remove residual ions and dried at 60 °C in air for 12 h for further characterization.

2.2. Photocatalytic activities measurements

The photocatalytic activity of the samples was evaluated by the degradation of Rhodamine B (50 mL, 20 mg L^{-1}), salicylic acid (50 mL, 20 mg L^{-1}) and phenol (50 mL, 2mg L^{-1}) under visible light and UV light irradiation, respectively, using a 350 W Xe lamp with a 420 nm and 365 nm cutoff filter. In each experiment, 50 mg of catalysts was suspended in aqueous solution. The suspensions were magnetically stirred in the dark for 1 h to ensure the establishment of an adsorption/desorption equilibrium between the organics and the catalyst, then the suspensions were vertically irradiated. At given irradiation time intervals, 3 mL solution was sampled, centrifuged, and then filtered through a Millipore filter (pore size 0.45 μm) to remove the catalyst particulates. The concentration of RhB and salicylic acid was analyzed by the UV–vis spectrometer measurement (UV-2550, Shimadzu).

Phenol in the reaction solution was analyzed on a Dionex high performance liquid chromatography (HPLC) instrument equipped with a Ultimate 3000 HPLC pump, Ultimate 3000 Diode Array Detector, and a Acclaim™ 120C18 reverse column (4.6 mm × 250 mm, particle size 5 μm, 120 Å). The mobile phase was 60% methanol and 40% water with a flow rate of 1 mL min^{-1} and the detection wavelength of phenol was 211 nm.

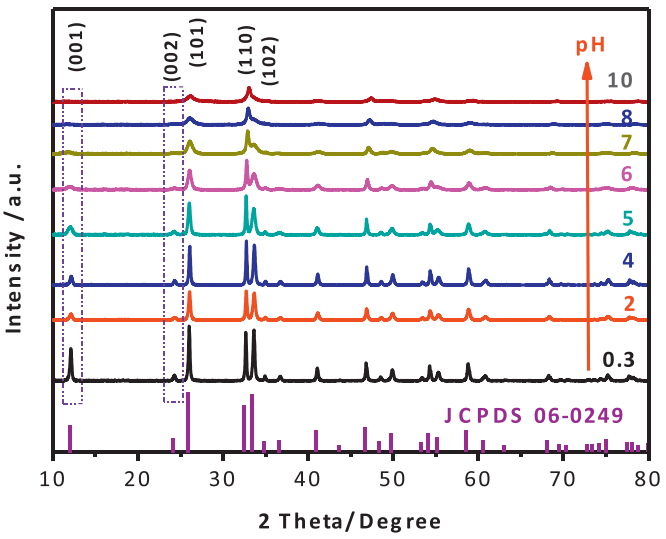

Fig. 1. XRD patterns of the as-prepared BiOCl products at different pH values.

2.3. Characterizations

The crystalline structure of the catalysts was characterized by powder X-ray diffraction (XRD) (Bruker D8 Advance; Cu Kα = 1.5404 Å). The XRD pattern was recorded within 2θ range from 10° to 80° at a scanning rate of 0.05°/s. The morphologies and particle sizes of the samples were observed by an SU8000 field-emission scanning electron microscope (FESEM, Hitachi, Japan) at an accelerating voltage of 15 kV. Energy dispersive spectrum analysis (EDS) system was connected to the SEM. Transmission electron micrograph (TEM) using a Tecnai G20 (FEI Co., Holland) microscope operated at accelerating voltage of 200 kV. The sample was prepared by dispersing the powder in ethanol and dropping a drop of very dilute suspension onto a carbon film-coated copper grid. X-ray photoelectron spectroscopy (XPS) measurements were conducted on a VG Multilab 2000 (VG Inc.) photoelectron spectrometer using Al Kα radiation as the excitation source under vacuum at 2×10^{-6} Pa. All the binding energy (BE) values were calibrated by the C 1s peak at 284.6 eV of the surface adventitious carbon. UV–vis diffused spectrum (DRS) was measured using the diffuse reflectance method with a Shimadzu UV-2550 spectrophotometer using an integrating sphere accessory. $BaSO_4$ was used as a reference materials in UV–vis diffuse experiments. The Brunauer–Emmett–Teller (BET) specific surface areas of the samples were evaluated on the basis of nitrogen adsorption isotherms using a Micromeritics ASAP 2020 gas adsorption apparatus (USA).

3. Results and discussion

The crystallographic structure and phase purity of the as-obtained sample were first examined by powder X-ray diffraction (XRD) analysis (Fig. 1). All the diffraction peaks could be easily indexed as the tetragonal phase of BiOCl with lattice constants of $a = b = 3.891$ Å, $c = 7.369$ Å (JCPDS card No.06-0249, space group P4/nmm). The effect of pH value on the crystalline phase was demonstrated through the changes of XRD patterns. With the increase of the pH value, all the diffraction peaks become increasing broad and the intensity of the (0 0 1) and (0 0 2) decrease gradually, indicating that the thickness of nanosheets becomes thinner with a small size along the [0 0 1] crystallographic direction [21]. We have also seen that with the increase of the pH value, the diffraction intensity ratio of (1 1 0)/(0 0 1) planes increase, which is attributed to the formation of ultrathin nanosheets oriented along the [0 0 1] direction [17,22].

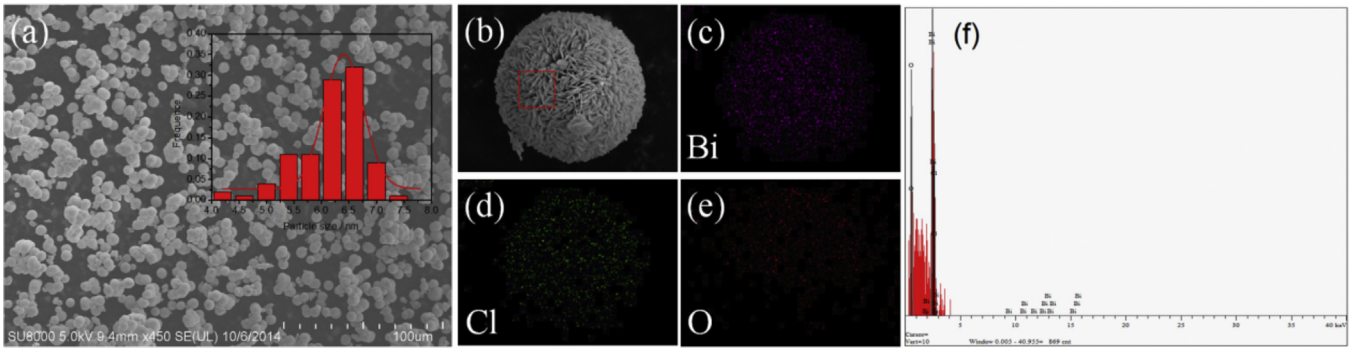

Fig. 2. (a) The low-magnification SEM image of BiOCl hierarchical microsphere and particle size distribution (inset), (b) high-magnification SEM image of a single BiOCl sample, (c–e) chemical element mapping images, (f) EDS data.

Table 1
BET surface area and pore volume of the as-synthesized samples at different pH value.

	pH 0.3	pH 5	pH 7	pH 8
S_{BET} (m^2/g)	9.3	18.8	26.4	31.7
V_{BJH} (cm^3/g)	0.06	0.13	0.1	0.1

The morphology and structure of the as-obtained phase-pure BiOCl were characterized by scanning electron microscopy (SEM) and transmission electron microscopy (TEM). It can be seen that the pH values have a significant influence on the thickness of the final products. As can be seen from its overall view (Fig. 2a), the products are uniform spherical in shape with a rather narrow size distribution of about 6.5 μm. The close-up view of an individual sphere (Fig. 2b) indicates that the sphere possess a superstructure assembled by numerous thin nanosheets with the thickness of about 30 nm. Chemical element mapping analysis (Fig. 2c–e) reveals that the elements including bismuth, chlorine and oxygen are homogenously distributed over the microsphere. The SEM–EDS area scans (Fig. 2f) further confirm the presence of Bi, Cl and O elements in the BiOCl microsphere, and the relative atom ratios are 36.7%, 46.5% and 42.2%, respectively, which are close to the BiOCl stoichiometry. In order to elucidate the significant influence of pH values on the thickness and microstructures, the products at different pH values were analyzed (Figs. 3 and 4). The products are also spherical in shape, but the sizes decrease from 6.5 μm to 3.5 μm in diameter (Fig. 3a–f). The high-magnification FESEM images of the samples (Fig. 4a–f) show that the BiOCl microspheres are assembled by densely BiOCl nanosheets with uniform width and thickness. We can see clearly that the higher the pH values, the thinner the thickness of BiOCl nanosheets. When the pH values are kept at 0.3 (Fig. 4a), the nanosheets are organized densely with a thickness of 30–50 nm. At pH 5 (Fig. 4c), we observe that the nanosheets becoming larger and thinner. The thickness of thin sheets is estimated to 10 nm and interweaves each other to form microsphere around a center. Interestingly, we are surprised to find that the nanosheets obtained at pH 8 and 10 is very thin, just like transparent wings. The thickness is less than 10 nm or even reaches 2–4 nm (Fig. 4e and f). Due to the thickness becomes thinner, most notable in the SEM images are the curly and twisted nanosheets, which increases the specific surface area tremendously (see Table 1). The TEM images further confirm that the BiOCl (obtained at pH 7) is microsphere composed of interweave nanosheets (Fig. 5a), and the width of nanosheets is about 100 nm (Fig. 5b), which is consistent with to

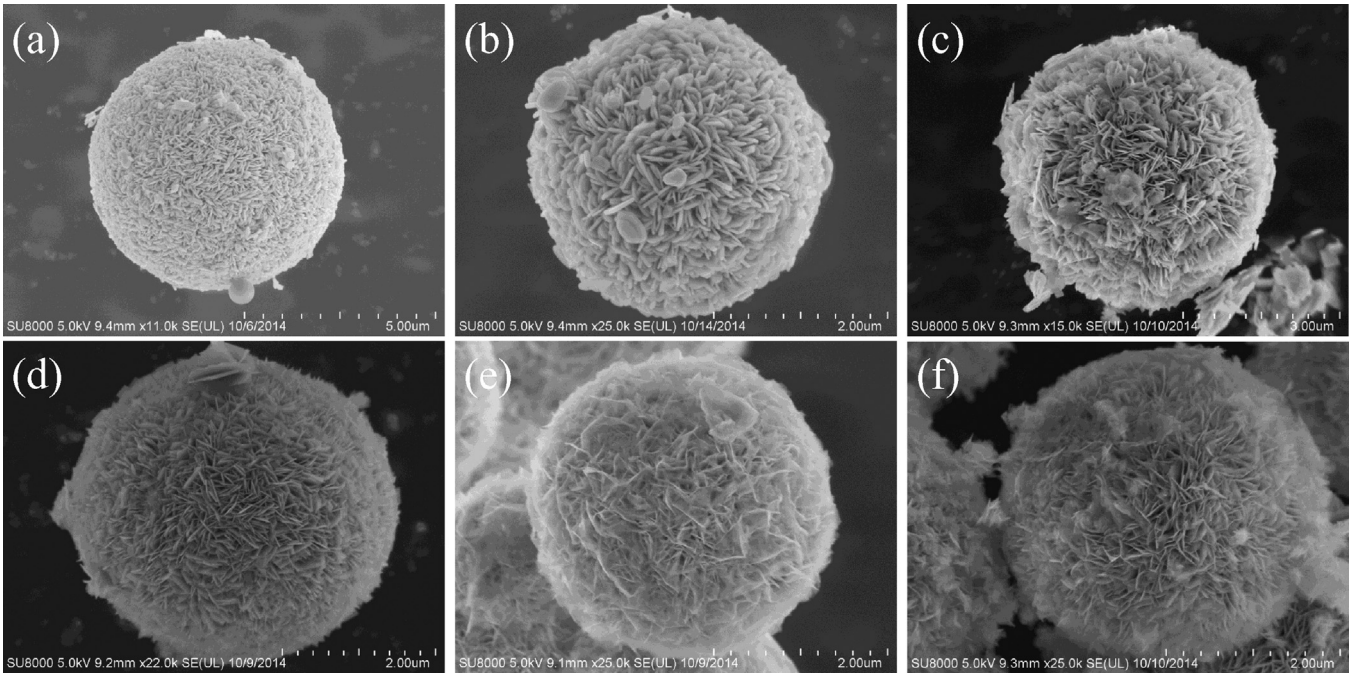

Fig. 3. SEM images of BiOCl hierarchical microsphere prepared at different pH values: (a) pH 0.3, (b) pH 2, (c) pH 5, (d) pH 7, (e) pH 8, (f) pH 10.

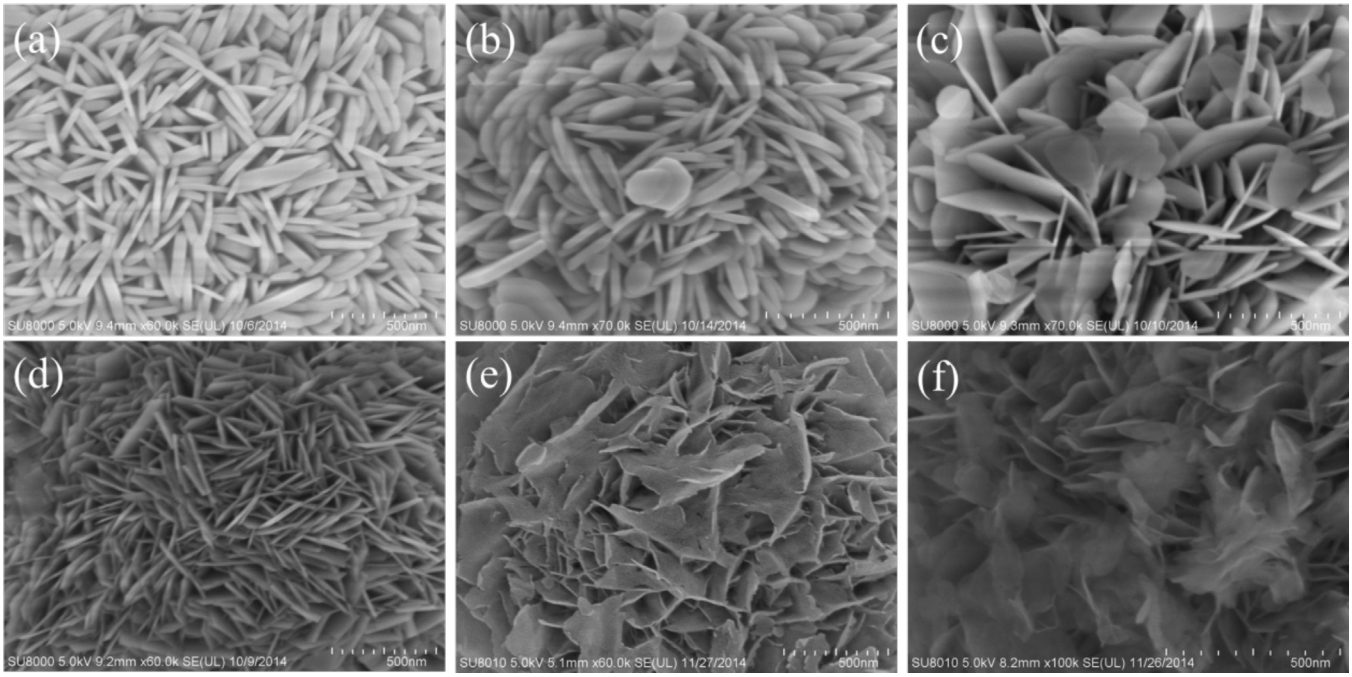

Fig. 4. Magnified SEM images of BiOCl hierarchical microsphere prepared at different pH values: (a) pH 0.3, (b) pH 2, (c) pH 5, (d) pH 7, (e) pH 8, (f) pH 10.

the previous SEM images. High-resolution TEM (HRTEM) images (Fig. 5c) reveal the highly crystalline nature of the nanosheets. The clear lattice fringes with an interplanar lattice spacing of 2.75 Å can be well matched to the (1 1 0) and (1-1 0) atomic planes. Obviously, (1 1 0) facet is perpendicular to (1-1 0) facet. Moreover, the angle labeled in the corresponding fast-Fourier transform (FFT) pattern (inset in Fig. 5c) is 45°, which is identical to the theoretical value of the angle between the (1 1 0) and (2 0 0) planes. The set of diffraction spots can be indexed as the [0 0 1] zone axis of tetragonal BiOCl [23]. All the above characterizations show that the BiOCl sheets with a preferred [0 0 1] orientation and the surface can be indexed as {0 0 1} facet (Fig. 5c).

We have known that bismuth nitrate is completely dissolved and swiftly formed intermediate species $[Bi_2O_2]^{2+}$ under acidic aqueous conditions [24]. Consequently, in our experiment, acetic acid as cosolvent facilitates an instant reaction between Bi^{3+}, water, and the halide anions, yielding the desired bismuth oxyhalide products as an easily separable precipitate, the formation mech-

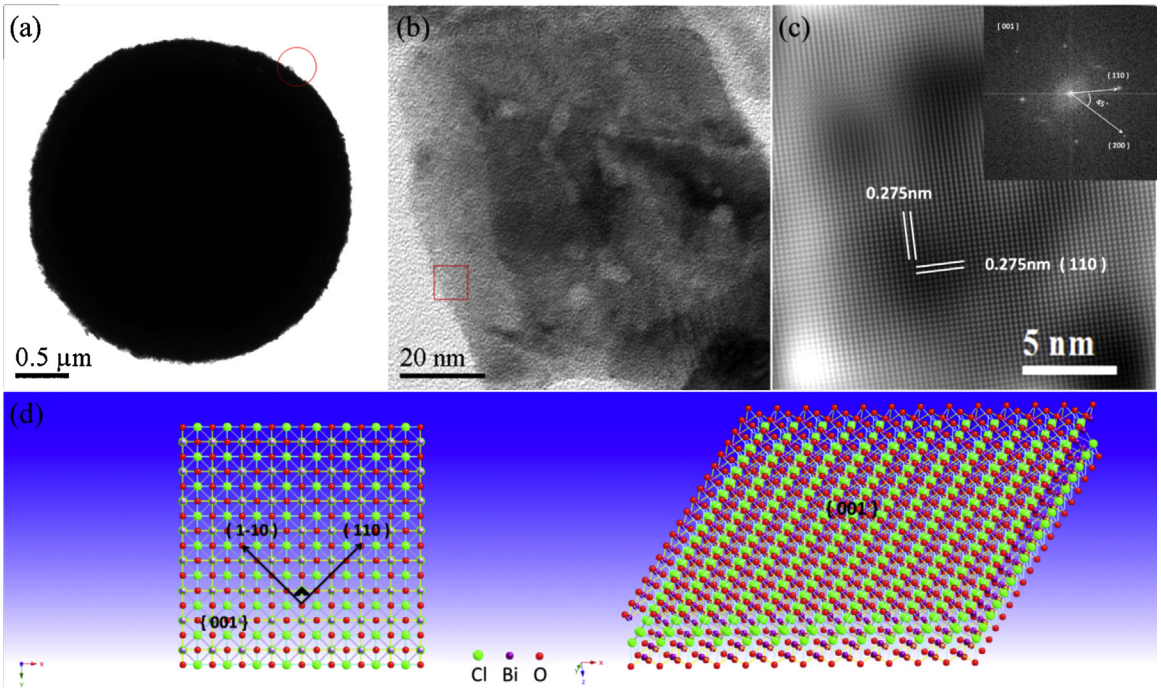

Fig. 5. TEM images of BiOCl hierarchical microsphere: (a) the low-magnification TEM image, (b) magnified TEM images, (c) the corresponding HRTEM image and the FFT patterns (inset), (d) the structure model illustration of BiOCl crystals.

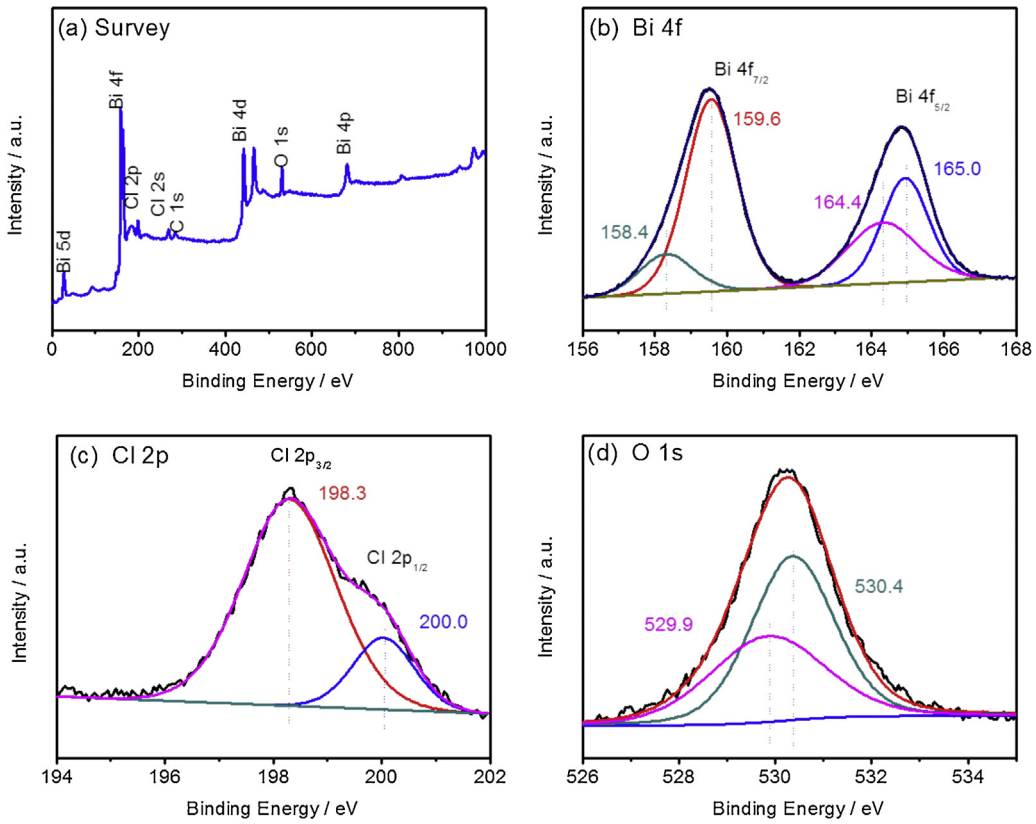

Fig. 6. XPS spectra of the BiOCl hierarchical microsphere (obtained at pH 5): (a) XPS survey pattern of the sample, (b) XPS spectrum of the Bi 4f region, (c) XPS spectrum of the Cl 2p region, (d) XPS spectrum of the O 1s region.

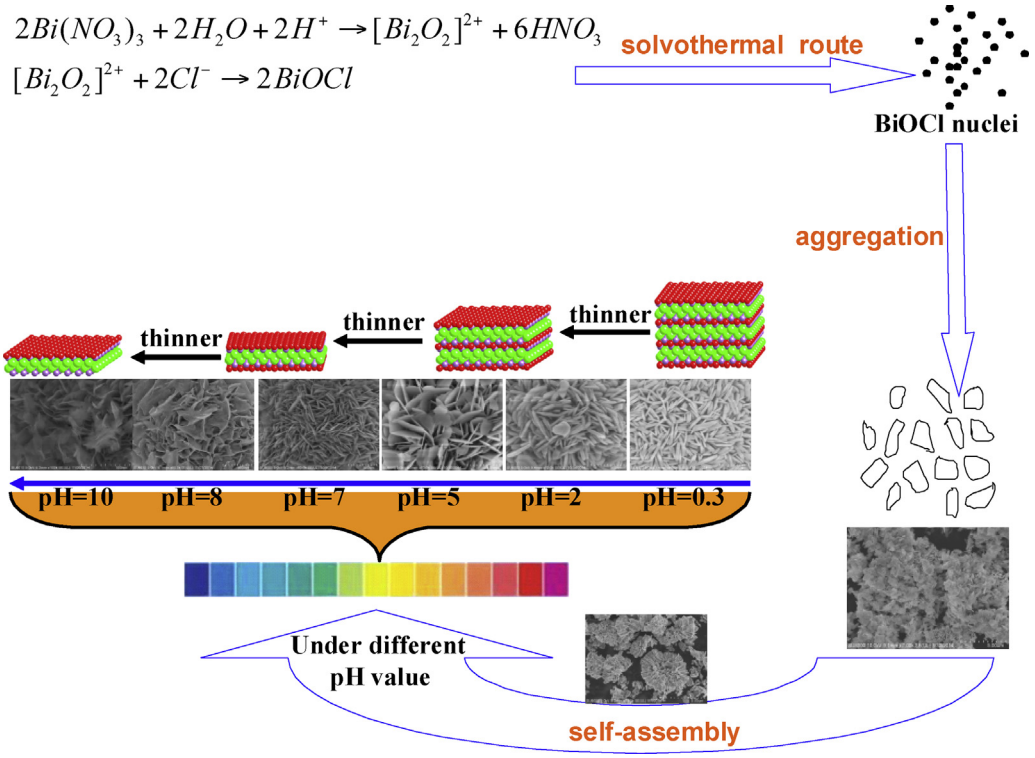

Scheme 1. Schematic illustration of proposed formation mechanism of BiOCl hierarchical microsphere.

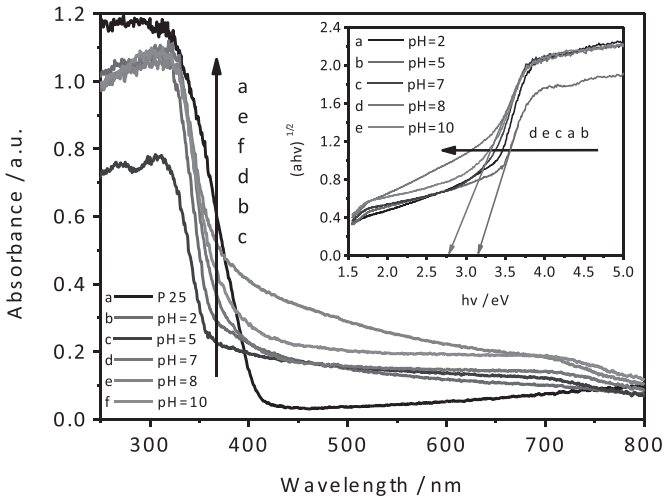

Fig. 7. UV–vis diffuse reflectance spectra of BiOCl hierarchical microsphere and plots of $(\alpha h\upsilon)^{1/2}$ versus photon energy $(h\upsilon)$ of BiOCl samples.

anism can be understood with the following reactions (Eqs. (1) and (2)) [25].

$$2Bi(NO_3)_3 + 2H_2O + 2H^+ \rightarrow [Bi_2O_2]^{2+} + 6HNO_3 \quad (1)$$

$$[Bi_2O_2]^{2+} + 2Cl^- \rightarrow 2BiOCl \quad (2)$$

Additional experiments were conducted in order to examine whether the reaction time and reaction temperature also played an important role in controlling the thickness and microstructures. The corresponding products were examined by XRD and SEM. As the reaction time was prolonged or reaction temperature was increased, the width of the diffraction peaks was unchanged, but the intensities increased gradually (Figs. S2 and S3), indicating that a better crystalline phase formed. As can be seen (Figs. S4 and S5), there is not a significant change on the thickness of the nanosheets under different reaction time and reaction temperature, which means the reaction time and reaction temperature have little effect on the thickness and microstructures.

Based on the above results, we believe that the pH value really has a momentous influence on the crystal growth of the BiOCl hierarchical microsphere. A possible formation process is schematically illustrated in Scheme 1. At the beginning, the

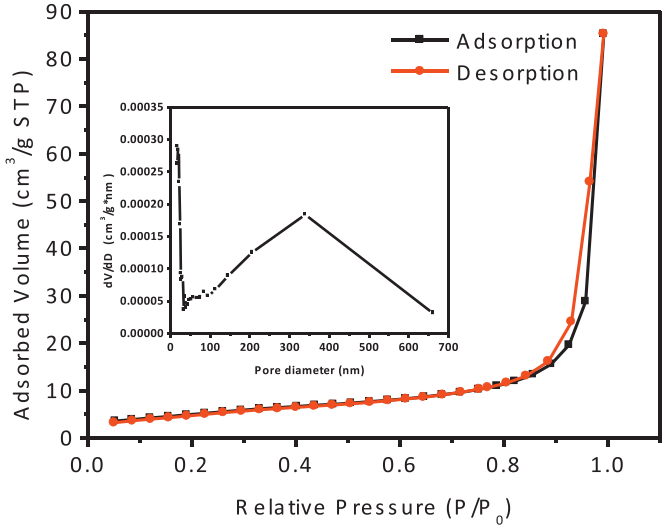

Fig. 8. Nitrogen adsorption–desorption isotherms of BiOCl (obtained pH 5). The inset shows BJH pore-size distributions.

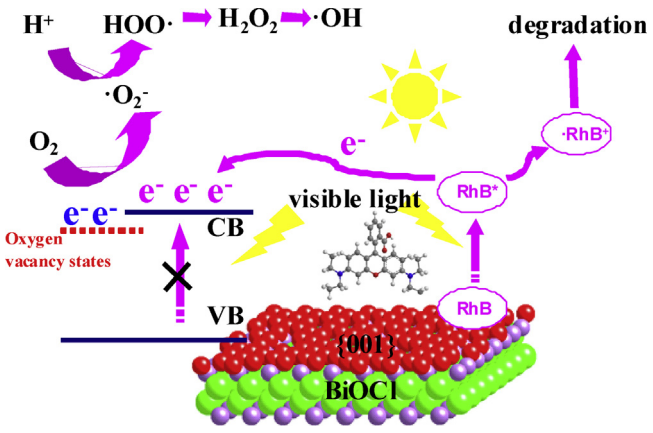

Scheme 2. Proposed mechanism for visible-light-driven photocatalytic degradation of RhB over BiOCl.

reagents are added into the reaction system, with large amounts of nuclei of BiOCl formed. Because of the special spatial structure of BiOCl, these nuclei grow and transform into the 2D nanosheets. With the pH value variation in the system, different thickness nanosheets are obtained. Subsequently, these 2D nanosheets are oriented-aggregate and then self-assembly into 3D BiOCl hierarchical microspheres. During the process, acetic acid is used as cosolvent to facilitate the dissolution of bismuth nitrate and H^+ ions are easily adsorbed on the O-terminated (0 0 1) surface of BiOCl nanoparticles to form of the {0 0 1} facets dominant BiOCl nanosheets. Further work is still needed to investigate the exact growth mechanism.

The XPS analysis was further carried out to analyze the chemical composition and elucidate the chemical state of the element in the BiOCl hierarchical microsphere (Fig. 6). The survey XPS spectrum of the sample contains the Bi, O, Cl, and C peaks (Fig. 6a). The C peak is mainly comes from the adventitious hydrocarbon of the XPS instrument itself. The high-resolution Bi 4f spectrum exhibits two individual peaks at 159.6 and 165.0 eV (Fig. 6b), assigned to the binding energies of Bi $4f_{7/2}$ and Bi $4f_{5/2}$ [26–28]. The additional peaks with lower binding energies at 158.4 and 164.4 eV, indicating the possibility appearance of $Bi^{(+3-x)}$ at the surface of BiOCl hierarchical microsphere, which may be due to a deficiency in oxygen and an enhanced concentration of oxygen vacancies in the vicinity

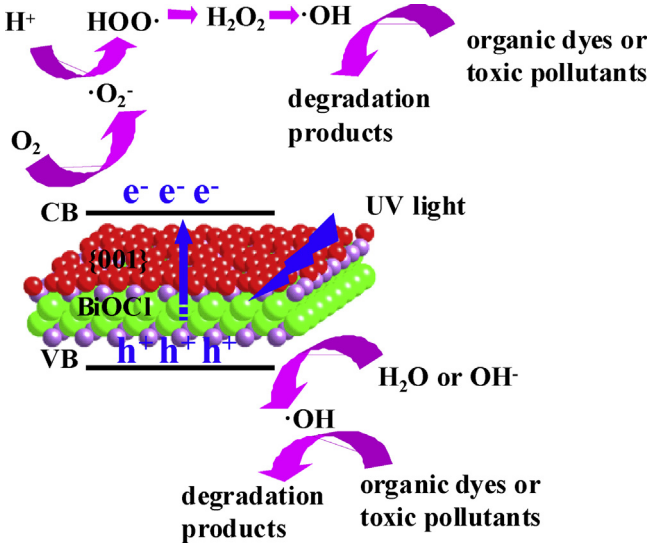

Scheme 3. Proposed mechanism for UV-light-driven photocatalytic degradation of organics over BiOCl.

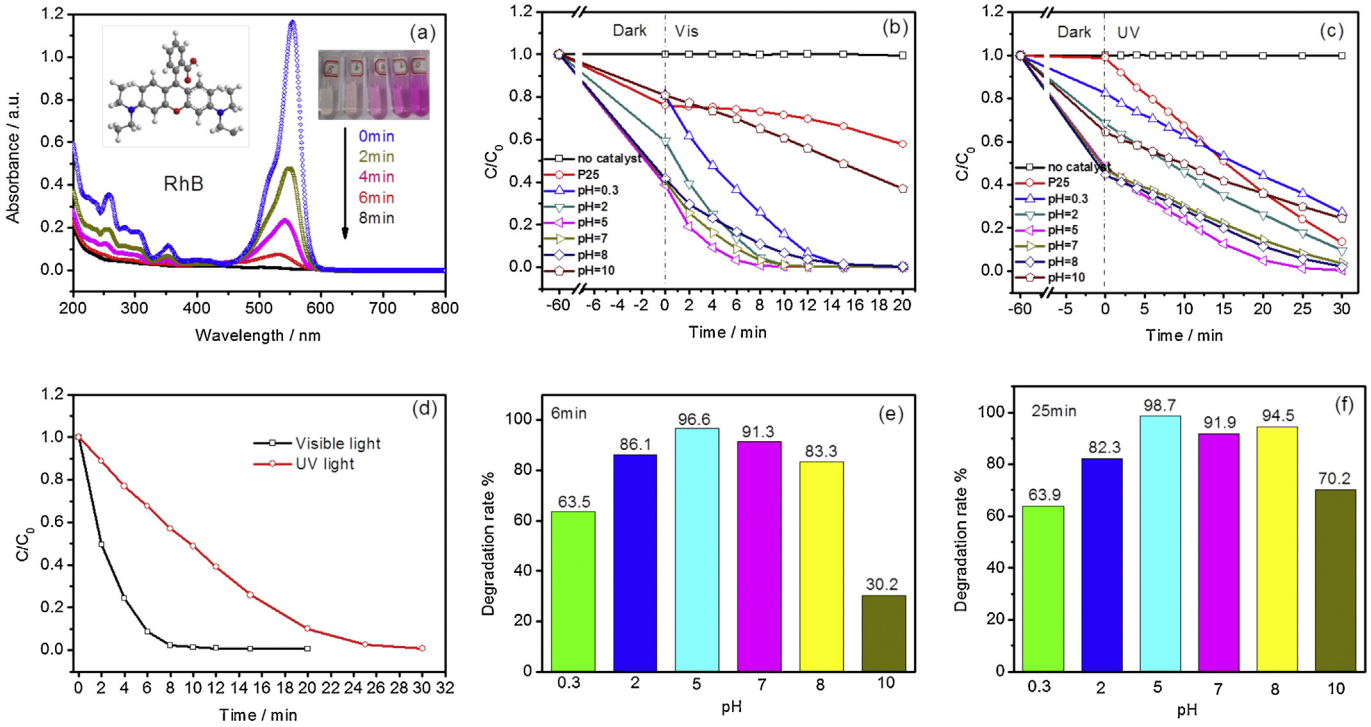

Fig. 9. (a) The temporal evolution of the absorption spectra of RhB (RhB: 20 mg L^{-1}) in the presence of the BiOCl samples (obtained at pH 5) under visible light irradiation (inset: the photo of time-dependent color change and the model of RhB). Photodegradation of RhB with different samples under (b) visible light and (c) UV light irradiation. (d) Comparison of photodecomposition of RhB with BiOCl hierarchical microsphere (obtained at pH 5) under UV and visible light irradiation. Comparative studies of RhB degradation rate under (e) visible light and (f) UV light irradiation over BiOCl samples obtained at different pH values.

of bismuth cations [29]. The Cl 2p spectrum is resolved into two peaks located at 198.3 and 200.0 eV (Fig. 6c), which are ascribed to the binding energies of Cl $2p_{3/2}$ and Cl $2p_{1/2}$, respectively [23]. Additionally, the O 1s peak at around 529.9 eV (Fig. 6d) is characteristic of O species in the Bi—O bonds of BiOCl lattice [30], and the O1s peak at 530.4 eV can be ascribed to the O species in surface hydroxyl groups absorbed on photocatalyst [31]. The higher intensity of the hydroxyl oxygen peak (around 530.4 eV) indicates that the BiOCl hierarchical microsphere (obtained at pH 5) possesses a higher concentration of surface adsorbed OH group, which may be favorable for photocatalytic reactions.

It is well known that the optical absorption properties of the semiconductor materials play a significant role in the photosensitization activity. Thus, the UV–vis absorption spectra of BiOCl hierarchical microsphere were measured by UV–vis diffuse reflectance spectroscopy in the wavelength range of 250–800 nm (Fig. 7). For crystalline semiconductors, the optical absorption near the band edge follows the equation [32]: $\alpha h\upsilon = A(h\upsilon - E_g)^{n/2}$ where α, υ, A and E_g are the absorption coefficient, light frequency, proportionality constant and optical band-gap energy, respectively. Among them, n depends on the characteristics of the transition in a semiconductor whether the transition is direct ($n = 1$) or indirect ($n = 4$). In our experiment, a strong absorption in the UV-light region around 387 nm can be assigned to the intrinsic band gap absorption of BiOCl. We also present P25 for comparison. By extrapolating the linear portion of the $(\alpha h\upsilon)^{1/2}$ versus $h\upsilon$ curves to the energy axis at $\alpha = 0$, the wide-band gap of the BiOCl hierarchical microsphere (obtained at pH 5) is estimated to be 3.2 eV. The band gaps of BiOCl hierarchical microsphere synthesized with different pH values, ranging from 2.8 eV to 3.2 eV. We observe the absorption edge of the BiOCl hierarchical microsphere (obtained at pH 8) located at about 400 nm in the near-UV region, which exhibits obvious red-

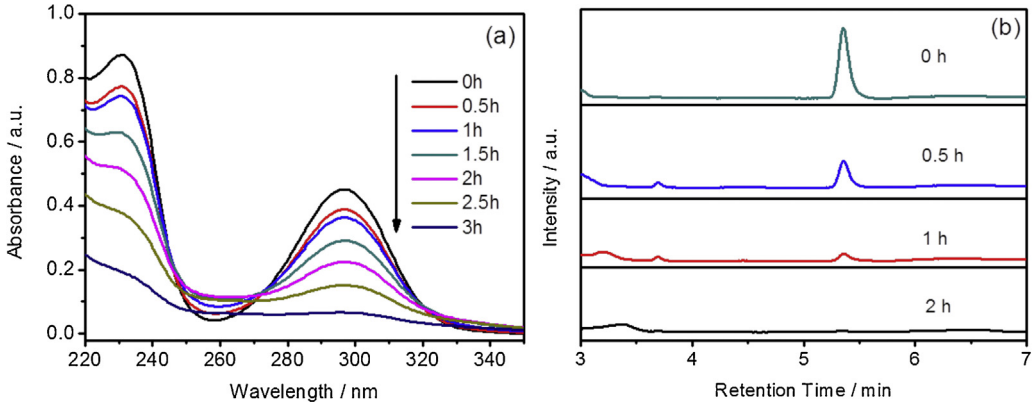

Fig. 10. (a) UV–vis spectra of salicylic acid catalyzed by BiOCl (obtained at pH 5) under UV light irradiation. (b) High-performance liquid chromatography (HPLC) analysis of phenol photodegradation over BiOCl (obtained at pH 5) under UV light irradiation.

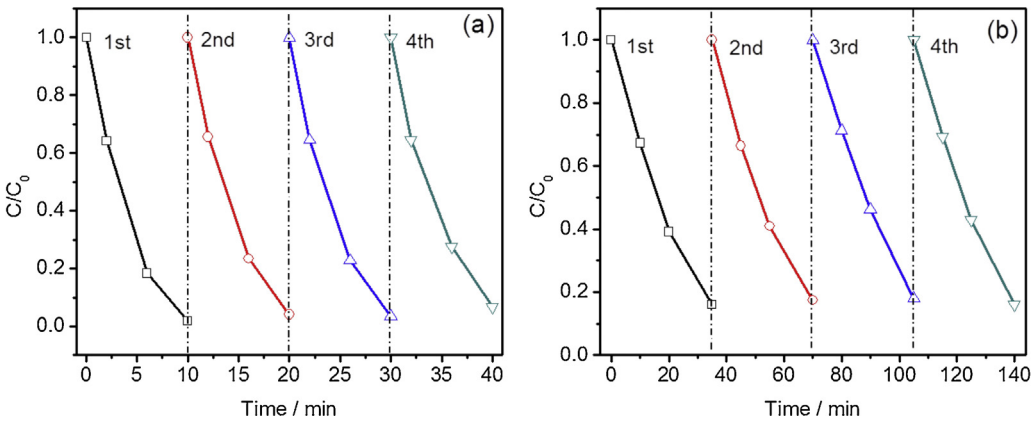

Fig. 11. Photocatalytic degradation of RhB by BiOCl hierarchical microsphere in repeated experiments under (a) visible light and (b) UV light irradiation.

shifts compared with previous report [17,18]. It may be due to the presence of oxygen vacancies [33], resulting in the higher quantum efficiency of photocatalysis. These experiment results indicate that the improvement of absorption ability is related to the thickness of a sheet.

The microporous structures and specific surface areas of BiOCl hierarchical microspheres were further studied by the nitrogen adsorption–desorption experiment (Fig. 8 and Fig. S6). All the BiOCl samples display type II adsorption–desorption isotherms, which are typical characteristics of macroporous materials [34]. These macropores are believed to be produced by interaggregated nanosheets. This can be confirmed by the previous results of SEM images. The BET specific surface areas of BiOCl hierarchical microsphere at different pH value are quite different. The sample at pH 8 has a larger BET surface of 31.7 m^2/g, but at pH 5 has a larger pore volume of 0.13 cm^3/g. More detailed information is summarized in Table 1. As far as we know, the BET surface area of all the samples is much larger than that in the literature [35–37]. It is well-known that large surface areas are beneficial to the adsorption of RhB. These unique structures may result in a high photocatalytic activity.

The photocatalytic degradation of organic dyes or toxic pollutants is widely used to characterize the activity of photocatalysts, which is of great significance in environmental pollutant treatment. The photocatalytic activity of BiOCl hierarchical microsphere was evaluated under visible light and UV light irradiation using Rhodamine-B (RhB). As we known, the RhB characteristic absorption peak is at 553 nm (location of RhB chromophore). As shown in Fig. 9a, with the irradiation time go on, the peak declines promptly. After 8 min, it nearly vanishes. As the diminishment of the peak at 553 nm, the peaks around at 354 and 258 nm gradually declines which suggests that it is a mineralization process accompanying the destruction of the conjugated structure of RhB [23]. Photodegradation of RhB with different samples under visible light and UV light irradiation are shown in Fig. 9b and c. As a comparison, commercial P25 was also performed under the same conditions, the BiOCl hierarchical microspheres showed higher activities for the RhB degradation than commercial P25 both under visible light and UV light irradiation. Compared the degradation rate under visible light irradiation 6 min and UV light irradiation 25 min at different pH value (Fig. 9e and f), the photocatalytic activity increases with decreasing pH value from 0.3 to 5, than decreases again with pH value from 5 to 10. The samples obtained at pH 5 exhibited the highest photocatalytic activity, 96.6% and 98.7% of RhB was degraded under visible light and UV light irradiation. We also compared photocatalytic performance of BiOCl hierarchical microsphere under visible light and UV light irradiation. The result was shown in Fig. 9d, the photocatalytic reactivity of BiOCl hierarchical microsphere under visible light is higher than under UV light. In other words, the indirect dye photosensitization superior to direct semiconductor photoexcitation in the BiOCl hierarchical microsphere. It is well known that a dye photosensitization mechanism is closely related to the dye absorbance and the adsorption capability of photocatalyst. Under the irradiation of visible light, the BiOCl hierarchical microspheres could not be excited and RhB acted as a photosensitizer [38]. However, the BiOCl played a key roles serve as electron carriers and electron acceptors. The detailed generation and transfer of photogenerated carriers in the indirect dye photosensitization pathways are shown in Scheme 2. The oxygen atom density on the {001} facets of BiOCl is much high, which is responsible for the high adsorption of RhB on the surface of BiOCl [39]. The exposed oxygen atom density could also cause a greater oxygen vacancy concentration, which could induce the second transfer of electrons, promoting the photosensitization activity.

Due to BiOCl only be active by UV light, other colorless pollutant salicylic acid and phenol are also used to investigate the photocatalytic performance of BiOCl. And Fig. 10a shows its UV–vis spectra change versus time, salicylic acid can be decomposed in 3 h indicating the BiOCl hierarchical microspheres obtained at pH 5 indeed has high photocatalytic activity. Fig. 10b shows that the very symmetrical peak of phenol in the start of the reaction decreased gradually and nearly disappears after 2 h. But we did not observed any new peaks appeared with the exposure time progresses, the intermediates or photodegradation products had not been detected under this detection condition [40]. It also can be seen that the decomposition of organic pollutants phenol under UV light irradiation is rapid and efficient. The detailed generation and transfer of photogenerated carriers in the direct semiconductor photoexcitation pathways are shown in Scheme 3.

To examine the stability of the BiOCl hierarchical microspheres, the photocatalyst for the photodegradation of RhB was reused and recycled, and the results are shown in Fig. 11. It can be seen that the BiOCl hierarchical microspheres still maintain relatively consistent photocatalytic activity after four recycles under both visible light and UV light irradiation. XRD patterns (Fig. S7) and SEM images (Fig. S8) also show that no significant change in the crystalline structure and morphological features after four recycles. Thus, these BiOCl hierarchical microspheres can work as an efficient and durable photocatalyst.

5. Conclusions

In summary, we have synthesized uniform BiOCl hierarchical microspheres via a simple solvothermal route. Each microsphere is composed of nanosheets with tunable thickness. The thickness of nanosheets can be controlled by adjusting the pH values. Under

visible light irradiation, the BiOCl hierarchical microspheres obtained at pH 5 show highest activity for dye photosensitization degradation of RhB, which is much superior to that of Degussa P25. The high photodecomposition activity can be attributed to the high specific surface area and oxygen vacancies concentration in the surface of the ultrathin nanosheets. And under UV light irradiation, the BiOCl hierarchical microspheres also show high photocatalytic performance for the direct semiconductor photoexcitation degradation of salicylic acid and phenol. This work may open a novel strategy to controllable synthesis of BiOCl nanomaterials with high photocatalytic performance.

Acknowledgement

This work was supported by Natural Science Foundation of Hubei Province (2013CFA089).

Appendix A. Supplementary data

Supplementary data associated with this article can be found, in the online version, at http://dx.doi.org/10.1016/j.apcatb.2015.02.019.

References

[1] T.F. Zhou, J.C. Hu, Environ. Sci. Technol. 44 (2010) 8698–8703.
[2] H.L. Wang, L.S. Zhang, Z.G. Chen, J.Q. Hu, S.J. Li, Z.H. Wang, J.S. Liu, X.C. Wang, Chem. Soc. Rev. 43 (2014) 5234–5244.
[3] G.Q. Zhang, X.W. Lou, Sci. Rep. 3 (2013) 1470.
[4] T.F. Zhou, W.K. Pang, C.F. Zhang, J.P. Yang, Z.X. Chen, H.K. Liu, Z.P. Guo, ACS Nano 8 (2014) 8323–8333.
[5] S.U.M. Khan, M. Al-Shahry, W.B. Ingler, Science 297 (2002) 2243–2245.
[6] W.Q. Fang, Z.Y. Huo, P.R. Liu, X.L. Wang, M. Zhang, Y. Jia, H.M. Zhang, H.J. Zhao, H.G. Yang, X.D. Yao, Chem. Eur. J. 20 (2014) 11439–11444.
[7] S.N. Zhang, S.J. Zhang, L.M. Song, Appl. Catal. B: Environ. 152–153 (2014) 129–139.
[8] J.G. Yu, J.X. Low, W. Xiao, P. Zhou, M. Jaroniec, J. Am. Chem. Soc. 136 (2014) 8839–8842.
[9] J.G. Hou, Z. Wang, C. Yang, W.L. Zhou, S.Q. Jiao, H.M. Zhu, J. Phys. Chem. C 117 (2013) 5132–5141.
[10] H. Liu, M. Luo, J.C. Hu, X.L. Zhou, J.L. Li, Sci. Adv. Mater. 5 (2013) 1–11.
[11] W.J. Zhou, Z.Y. Yin, Y.P. Du, X. Huang, Z.Y. Zeng, Z.X. Fan, H. Liu, J.Y. Wang, H. Zhang, Small 9 (2013) 140–147.
[12] D.W. Ding, K. Liu, S.N. He, C.B. Gao, Y.D. Yin, Nano Lett. 14 (2014) 6731–6736.
[13] L.A. Gu, J.Y. Wang, H. Cheng, Y.Z. Zhao, L.F. Liu, X.J. Han, ACS Appl. Mater. Interfaces 5 (2013) 3085–3093.
[14] J. Tian, Y.H. Sang, G.W. Yu, H.D. Jiang, X.N. Mu, H. Liu, Adv. Mater. 25 (2013) 5075–5080.
[15] X. Zhang, Z.H. Ai, F.L. Jia, L.Z. Zhang, J. Phys. Chem. C 112 (2008) 747–753.
[16] K.L. Zhang, C.M. Liu, F.Q. Huang, C. Zheng, W.D. Wang, Appl. Catal. B: Environ. 68 (2006) 125–129.
[17] D.H. Wang, G.Q. Gao, Y.W. Zhang, L.S. Zhou, A.W. Xu, W. Chen, Nanoscale 4 (2012) 7780–7785.
[18] J. Jiang, K. Zhao, X.Y. Xiao, L.Z. Zhang, J. Am. Chem. Soc. 134 (2012) 4473–4476.
[19] M.L. Guan, C. Xiao, J. Zhang, S.J. Fan, R. An, Q.M. Cheng, J.F. Xie, M. Zhou, B.J. Ye, Y. Xie, J. Am. Chem. Soc. 135 (2013) 10411–10417.
[20] H.F. Cheng, B.B. Huang, Y. Dai, Nanoscale 6 (2014) 2009–2026.
[21] (a) W.Q. Fang, J.Z. Zhou, J. Liu, Z.G. Chen, C. Yang, C.H. Sun, G.R. Qian, J. Zou, S.Z. Qiao, H.G. Yang, Eur. J. Chem. 17 (2011) 1423–1427;
(b) Y. Xu, S.C. Xu, S. Wang, Y.X. Zhang, G.H. Li, Dalton Trans. 43 (2014) 479–485.
[22] X.H. Yang, Z. Li, G. Liu, J. Xing, C.H. Sun, H.G. Yang, C.Z. Li, CrystEngComm 13 (2011) 1378–1383.
[23] J.L. Hu, W.J. Fan, W.Q. Ye, C.J. Huang, X.Q. Qiu, Appl. Catal. B: Environ. 158–159 (2014) 182–189.
[24] Z. Jiang, F. Yang, G.D. Yang, L. Kong, M.O. Jones, T.C. Xiao, P.P. Edwards, J. Photochem. Photobiol. A 212 (2010) 8–13.
[25] H. Gnayem, Y. Sasson, ACS Catal. 3 (2013) 186–191.
[26] Y. Yu, C.Y. Cao, H. Liu, P. Li, F.F. Wei, Y. Jiang, W.G. Song, J. Mater. Chem. A 2 (2014) 1677–1681.
[27] G. Cheng, J.Y. Xiong, F.J. Stadler, New J. Chem. 37 (2013) 3207–3213.
[28] J. Jiang, L.Z. Zhang, H. Li, W.W. He, J.J. Yin, Nanoscale 5 (2013) 10573–10581.
[29] S.M. Zhang, G.K. Zhang, S.J. Yu, X.G. Chen, X.Y. Zhang, J. Phys. Chem. C 113 (2009) 20029–20035.
[30] F.X. Xie, X.M. Mao, C.M. Fan, Y.W. Wang, Mat. Sci. Semicon. Proc. 27 (2014) 380–389.
[31] L. Armelao, G. Bottaro, C. Maccato, E. Tondello, Dalton Trans. 41 (2012) 5480–5485.
[32] M.A. Butler, J. Appl. Phys. 48 (1977) 1914–1920.
[33] K. Zhao, L.Z. Zhang, J.J. Wang, Q.X. Li, W.W. He, J.J. Yin, J. Am. Chem. Soc. 135 (2013) 15750–15753.
[34] J.X. Xia, S. Yin, H.M. Li, H. Xu, Y.S. Yan, Q. Zhang, Langmuir 27 (2011) 1200–1206.
[35] J.M. Song, C.J. Mao, H.L. Niu, Y.H. Shen, S.Y. Zhang, CrystEngComm 12 (2010) 3875–3881.
[36] J.Y. Xiong, G. Cheng, G.F. Li, F. Qin, R. Chen, RSC Adv. 1 (2011) 1542–1553.
[37] X. Zhang, X.B. Wang, L.W. Wang, W.K. Wang, L.L. Long, W.W. Li, H.Q. Yu, ACS Appl. Mater. Interfaces 6 (2014) 7766–7772.
[38] G.S. Li, B. Jiang, S.N. Xiao, Z.C. Lian, D.Q. Zhang, J.C. Yu, H.X. Li, Environ. Sci.: Process. Impacts 16 (2014) 1975–1980.
[39] L.Q. Ye, L. Zan, L.H. Tian, T.Y. Peng, J.J. Zhang, Chem. Commun. 47 (2011) 6951–6953.
[40] Z.P. Wang, W.M. Cai, X.T. Hong, X.L. Zhao, F. Xu, C.G. Cai, Appl. Catal. B: Environ. 57 (2005) 223–231.